Journal of The Electrochemical Society, 2023 **170** 063502

Continuous Purification of Molten Chloride Salt: Electrochemical Behavior of MgOHCl Reduction

Liam Witteman,[1,2,3,*] Kerry Rippy,[2,3,z] Patrick Taylor,[3] and Judith Vidal[2,3]

[1]*Advanced Energy System Program, Colorado School of Mines, Colorado, United States of America*
[2]*National Renewable Energy Laboratory, Colorado, Golden, United States of America*
[3]*Kroll Institute for Extractive Metallurgy, Colorado School of Mines, Colorado, United States of America*

We present a study on the electrochemical behavior of magnesium hydroxide ($MgOH^+$) reduction on a tungsten (W) cathode in molten chloride salt ($MgCl_2$-KCl-NaCl) across the temperature range of 475 °C–525 °C. $MgOH^+$, which forms within the salt upon exposure to moisture, is a leading cause of corrosion. Corrosion is a major barrier to deployment of chloride salts across a number of applications, including concentrating solar power plants and nuclear power plants. While pre-purification protocols have been developed to ensure $MgOH^+$ is removed from molten chloride salts prior to deployment, $MgOH^+$ forms in situ during operation of chloride-salt based plants. Thus, methods for continuous purification during plant operation are needed. Continuous electrochemical purification via electrolysis using a Mg anode and W cathode has been proposed, but little has been done to assess scalability. Here, we assess fundamental properties of electrochemical removal of $MgOH^+$ to enable future scale up of this method.
 [DOI: 10.1149/1945-7111/acd878]

Manuscript submitted January 3, 2023; revised manuscript received May 3, 2023. Published June 2, 2023. *This paper is part of the JES Focus Issue on Molten Salts and Ionic Liquids III.*

Molten chloride salts have been identified as prime heat transfer fluids and thermal energy storage media in the next generation of concentrating solar power (CSP) and nuclear plants.[1–12] Particularly, a Mg-K-Na chloride blend (45.98–38.91–15.11 wt%) has received significant attention due to its low cost, widespread availability, and favorable thermohydraulic properties.[13–16] However, $MgCl_2$ readily hydrolyzes to form corrosive MgOHCl.[17–24] Events such as leaks and maintenance in the salt loop introduce air and moisture into the system and increase levels of MgOHCl. Therefore, a purification process that operates continuously in flowing molten chloride salt is desired to maintain acceptable MgOHCl levels.[15,25] An electrochemical purification process to remove MgOHCl has been demonstrated at the laboratory scale,[26] and results indicate significant opportunity for the electrochemical process to be scaled for industrial use. The aim of this work is to obtain key parameters and insight into the mechanism of an electrochemical purification process to aid in scale up and reactor design.

A vast body of literature exists on corrosion of alloys in molten chloride under various conditions and concentrations of MgOHCl.[27–37] An acceptable threshold of corrosion ($\leqslant 20\ \mu m\ year^{-1}$) can be obtained when MgOHCl concentration is 1000 ppm or less.[28,37] At these concentrations, corrosion was limited to $\sim 10\ \mu m\ year^{-1}$ and enabled the use of stainless steel instead of costly Ni super alloys.[37] Purification methods using Mg can successfully reach MgOHCl concentrations of $\leqslant$1000 ppm.[28,29] However, the use of Mg is only effective when the salt is heated to temperatures greater than 650 °C—the melting temperature of Mg. This poses a problem for the next generation of CSP and nuclear plants with sections of the salt loop operating at 500 °C.

An electrochemical purification method by Ding et al. demonstrated the feasibility of reaching 1000 ppm MgOHCl or less at 500 °C.[26] The authors removed MgOHCl ($MgOH^+$ in ionic form) via electrowinning using a W cathode and a Mg anode. Reactions (1–2) were hypothesized.

$$Cathode\text{: } MgOH^+ + e^- \rightarrow MgO + \frac{1}{2}H_2 \qquad [1]$$

$$Anode\text{: } \frac{1}{2}Mg \rightarrow \frac{1}{2}Mg^{2+} + e^- \qquad [2]$$

Understanding the process of Reactions (1–2) is needed to design an effective electrochemical purification reactor at commercial scale. Foremost, several key parameters must be determined for Reaction (1): the diffusion coefficient of $MgOH^+$, the standard rate constant, the charge transfer coefficient, and the number of electrons transferred. Furthermore, the process should be continuous for an industrial process; passivation of the electrode due to MgO formation would greatly hinder the kinetics of the process and demand frequent electrode replacement for cleaning unless in situ cleaning methods can be developed.

Ding et al. concluded that the W cathode passivated due to MgO formation on the electrode surface. Passivation is plausible given the low solubility of MgO in chloride salts such that any MgO formed would precipitate. The solubility of MgO has been reported to be 50 ± 25 ppm at 475 °C in molten $MgCl_2$-NaCl (41.5–58.5 mol%).[23] However, the current behavior in Ding et al. appeared to be diffusion limited, with a steady limiting current density of $125\ mA\ cm^{-2}$. Further work to determine passivation or diffusion as the cause is warranted. No other parameters of Reaction (1) were determined. Two studies were found with diffusion coefficients of $MgOH^+$, but none in the Mg-K-Na chloride blend of interest.[23,35] Furthermore, a discrepancy was found on the reduction potential associated with $MgOH^+$.[23,35,36,38]

In this study, we present the electrochemical behavior of $MgOH^+$ reduction on a W cathode in molten $MgCl_2$-KCl-NaCl across the temperature range of 475 °C–525 °C. First, the reduction potential of $MgOH^+$ was determined through cyclic voltammetry (CV) and analysis of the electrode surface for MgO via scanning electron microscope (SEM) and energy dispersive spectroscopy (EDS). Second, we present key parameters of Reaction (1), including diffusion coefficient of $MgOH^+$, charge transfer coefficient, standard rate constant, and number of electrons transferred. Last, we present the current behavior of a W cathode with and without the presence of convection. The extent of passivation was assessed by inspecting the electrode surface after two hours of electrolysis. The results in this study will aid in modeling and scaling a continuous electrochemical purification cell at industrially relevant scales.

Experimental

Preparation of salt mixture and heating procedure.—A ternary blend of chloride salts, $MgCl_2$ (45.98 wt%), KCl (38.91 wt%), NaCl

*Electrochemical Society Student Member.
[z]E-mail: kerry.rippy@nrel.gov

(15.11 wt%) was prepared in batches of 550 g.[16] $MgCl_2$ (99% Anhydrous, Alfa Aesar), KCl (≥99%, Avantor), and NaCl (≥99%, Fisher-Chemical) were used as received. The ternary blend was prepared and stored in an argon glovebox to avoid hydrolysis of $MgCl_2$ (≤0.5 ppm H_2O, ≤0.1 ppm O_2, Inert Technologies).

Salt was melted using the procedure adapted from Ding et al.[26] Prior to melting, the salt was put under vacuum (0.85 bar) for 30 min in the glovebox. The salt was then transferred to the reactor vessel and heated at a rate of 5 °C min^{-1} to 200 °C and held at temperature for 90 min. Afterwards, the salt was heated to the temperature of the experiments (475, 500, or 525 °C) at a rate of 5 °C min^{-1}. Throughout the heating procedure and experiments, ultra-high purity nitrogen (99.999%, ≤1 ppm H_2O, ≤1 ppm O_2) was flowed through the reactor at 100 ml min^{-1} to avoid moisture and oxygen ingress.

Experimental Setup

Figure 1 shows the experimental setup used for all experiments.

All experiments were conducted in a custom 8-port Pyrex reactor lid and vessel from Allen Scientific Glass Inc. The Pyrex reactor allowed visual observation of the salt and gas evolution during experiments. Within the Pyrex reactor, a fused quartz crucible (Advalue Technology) was used to hold the chloride salt mixture to avoid damage to the reactor vessel from the salt during cooling. A Pyrex thermocouple sheath with a k-type thermocouple (Omega Engineering) was directly inserted into the molten chloride salt to monitor the temperature set by a programmable furnace (Mellen). As noted, ultra-high purity nitrogen (99.999%, ≤1 ppm H_2O, ≤1 ppm O_2) flowed through the reactor at 100 ml min^{-1} to avoid moisture and oxygen ingress into the reactor. The cover gas outlet was passed through a 1.0 M NaOH scrubber, a desiccator column (Drierite), and a hydrogen gas analyzer (Midas-E-H2X, Honeywell) before exhausted. The NaOH scrubber was used to remove any potential HCl gas, and a desiccator was used to remove any moisture before passing through the hydrogen gas analyzer. The gas analyzer with a hydrogen gas cartridge measured H_2 gas between 0 and 1000 ppm within 10% error (calibrated with 500 ppm H_2 span gas).

In this work, a three-electrode setup was used for electrochemical experiments. An Ag/AgCl reference electrode was fabricated as described by Choi et al. and Wang et al.[38,39] A 0.5 mm diameter Ag wire (99.9%, AlfaAesar) was inserted into a 6.35 mm diameter alumina sheath (Advalue Technology). The bottom ~3 cm of the alumina sheath was polished down to ~15 μm wall thickness. Inside the alumina sheath 2.5 g of chloride salt mixture was added with 1 wt% of AgCl (99.9%, ThermoScientific). Table I summarizes the electrode materials used and the purpose of each experiment.

The W working electrodes were 1.49 mm in diameter. The W counter electrodes were 4.76 mm in diameter to ensure the working electrode was not surface area limited by the counter electrode. Similarly, the Mg counter electrode in CPC experiments was 7.85 mm in diameter. The W and Mg electrodes were purchased from Midwest Tungsten Service (99.95%) and Goodfellow (99.9%) respectively. Before each experiment, the electrodes were cleaned according to Ref. 40 to remove oxide film formation using 800, 1200, and 2000 grit sandpaper along with an alumina slurry (average particle size of 0.05 μm). After cleaning, the electrodes were stirred in 2% nitric acid solution for 1 min and then rinsed with de-ionized water. Once dry, the electrodes were immersed in the salt for at least one hour to ensure thermal equilibrium and a stable open-circuit potential (<0.5 mV s^{-1} drift).

All electrochemical experiments were conducted using a Gamry 1010 workstation. The potentiostat used in this study was not capable of positive feedback iR compensation. Therefore, the uncompensated resistance was measured via electrochemical impedance spectroscopy and found to be 0.1696 Ω. iR compensation was done post facto. Further details on post-facto correction are found in the theoretical section.

Determination of working electrode surface area.—The surface area of the electrode was calculated by physically measuring the immersion height via calipers after the experiment. This method has been demonstrated to be accurate within 0.5 mm for molten salts.[41] In our experiments the working electrode was typically immersed 2–3 cm, resulting in a calculated surface area error of less than 2%. Visual observation of the experiments confirmed no salt wicking up the electrodes.

Electrochemical cleaning of working electrode between measurements.—An electrochemical cleaning step was necessary

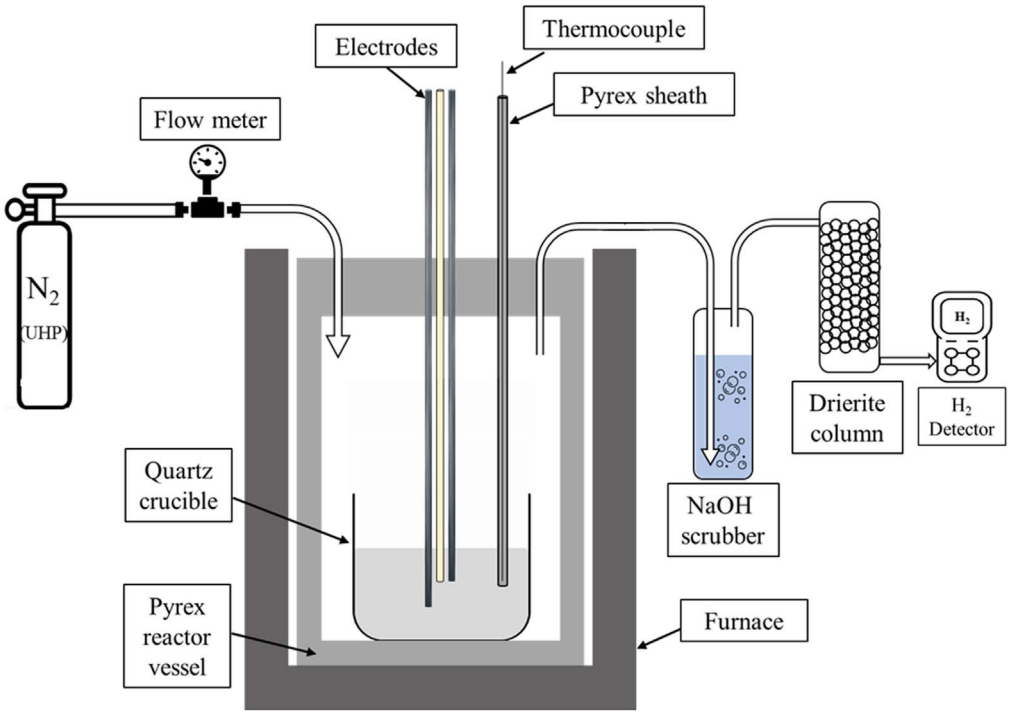

Figure 1. Schematic of experimental setup used in this study.

Table I. Electrode material for each experiment.

Method	Application	Electrode material		
		Working	Counter	Reference
Cyclic voltammetry (CV)	Determine reduction potential of $MgOH^+$ and standard rate constant.	W	W	Ag/AgCl
Controlled potential coulometry (CPC)	Determine mechanism of current behavior on cathode.	W	Mg	Ag/AgCl
Chronopotentiometry (CP)	Determine diffusion coefficient of $MgOH^+$, and charge transfer coefficient.	W	W	Ag/AgCl
Square wave voltammetry (SWV)	Determine number of electrons transferred.	W	W	Ag/AgCl

to obtain reproducible data, likely due to the formation of the insoluble product MgO on the working electrode. An electrochemical cleaning procedure was developed based on the work from Tylka et al.[42] The procedure is summarized in Table II.

The electrochemical cleaning procedure was optimized to minimize the anodic stripping step. The duration of step 2 was purposefully extended beyond the time required for a stable open circuit potential for convenience. This allowed for measurements to be obtained in 5 min intervals. The result of the electrochemical cleaning procedure resulted in repeatable cyclic voltammograms as shown in Fig. 2.

Figure 2 demonstrates the effectiveness of the electrochemical cleaning procedure to produce repeatable data given the near perfect overlap of 10 voltammograms. Based on ten scans, the 95% confidence interval of measured current density of the reduction peak at −0.65 V vs Ag/AgCl was only ±0.03 mA cm^{-2}.

Impurity doping of the salt.—To introduce MgOHCl impurity into the molten chloride salt mixture, NaOH pellets (∼1.0 g, ⩾97.0%, Macron) were directly added to the molten chloride salt mixture via an open reactor port according to Reaction (3).[35,36]

$$MgCl_2 + NaOH \rightarrow MgOHCl + NaCl \quad [3]$$

To ensure an accurate mass of NaOH, the pellets were dried overnight at 120 °C and stored in the glovebox until use. After NaOH introduction to the salt, Reaction (3) occurred rapidly as observed by the increase in current response in CV, and as measured via analysis with titration. Doping with MgOHCl was also explored but was not utilized because the dissolution of solid MgOHCl in the salt is slow (on the order of one hour).[23]

Calibration of cyclic voltammetry with acid-base titration.—Direct measurements of $MgOH^+$ via titration were necessary to enable the use of CV to quantify $MgOH^+$ in situ.[23,35,36] To relate the current density response from the $MgOH^+$ reduction peak requires calculating the multiplication factor $s_{CV}(T, v)$ (Eq. 4).

$$c_{MgOH^+} = j_{MgOH^+} \cdot s_{CV}(T, v) \quad [4]$$

Where $s_{CV}(T, v)$ is the multiplication factor as a function of temperature and scan rate (ppm O mA^{-1} cm^2), j_{MgOH^+} is the current density of the $MgOH^+$ reduction peak (mA cm^{-2}), and c_{MgOH^+} is the concentration of $MgOH^+$ in the salt (ppm), which can be found via acid-base titration.

To determine $s_{CV}(T, v)$, salt aliquots were taken immediately after a CV scan. The salt aliquots were drawn using a Pyrex tube attached to a handheld vacuum pump. The salt was stored under vacuum and then prepared for titration inside an argon glovebox.

To prepare the salt for titration, ∼0.5 g of salt was dissolved in 0.1 M nitric acid via stirring for 1 h at 500 rpm. The acid was then titrated with 0.05 M NaOH solution to calculate the total acid consumed. It was assumed all acid consumed was due to $MgOH^+$ given the low solubility of MgO in chloride salts (⩽50 ppm).[23,36]

The titrations for each aliquot were done in triplicates to report an average and a 95% confidence interval. The $s_{CV}(T, v)$ were determined and summarized in Table III.

From Table III, the values for $s_{CV}(T, v)$ decrease with increasing temperature as expected from literature.[23,36] Furthermore, $s_{CV}(T, v)$ at 500 °C agrees well with the value of 38.2 ± 7.2 obtained in Ref. 36.

Theoretical

Cyclic voltammetry behavior for soluble-insoluble reactions.—This section summarizes the mathematical models developed by Atek et al. and Krulic et al. for a soluble-insoluble system.[43,44] These models were built upon the work done by Berzins and Delahay to derive current- and potential-time behavior using the Nicholson-Shain model.[45,46] Additions to the model were made by accounting for deposition of product on a foreign substrate assuming instantaneous nucleation, and by accounting for uncompensated resistance. For further details the reader is suggested to visit Refs. 43, 44.

The first step is to develop a working curve using a reversibility factor defined as:

$$\omega = \frac{k^0}{\left(\frac{c_{MgOH^+}}{c_0}\right)^{\alpha_c}\left(\pi D_{MgOH^+}\frac{nF}{RT}v\right)^{1/2}} \quad [5]$$

Where k^0 is the standard rate constant of the reduction reaction (cm^2 s^{-1}), c_{MgOH^+} is the concentration of $MgOH^+$ (mol cm^{-3}), c_0 is the standard concentration (1 mol cm^{-3}), α_c is the cathodic charge transfer coefficient, F is Faraday's constant (96495 C mol^{-1}), n is the number of electrons transferred in the reaction, R is the ideal gas constant (8.314 J mol^{-1} K^{-1}), T is temperature (K), D_{MgOH^+} is the diffusion coefficient of $MgOH^+$ (cm^2 s^{-1}), and v is the scan rate (V s^{-1}).

The reversibility factor is analogous to the work done by Matsuda and Ayabe, but for soluble-insoluble reactions.[47] Reversibility is defined as $\omega \geqslant 10^3$ and irreversibility is defined as $\omega \leqslant 10^{-3}$. Intermediate values correspond to quasi-reversibility.[43]

For an electrochemically reversible reaction, the peak current density, j_p, and peak potential, E_p, can be modeled using Eqs. 6–8.

$$j_p = 0.6105 c_{MgOH^+}\sqrt{\frac{(nF)^3 D_{MgOH^+} v}{RT}} \quad [6]$$

$$E_p = E_i + \frac{RT}{nF}\ln(c_{MgOH^+}/c_0) - 0.854\frac{RT}{nF} \quad [7]$$

$$\Delta E_p = |E_p - E_{p/2}| = 0.774\frac{RT}{nF} \quad [8]$$

Where E_i is the initial potential where the wave starts (V), and $E_{p/2}$ is the peak potential at 0.5 j_p.

For an electrochemically irreversible redox reaction where the anodic process is considered negligible, Eqs. 9–11 are used:

$$j_p = 0.4958 c_{MgOH^+}\sqrt{\frac{\alpha_c (nF)^3 D_{MgOH^+} v}{RT}} \quad [9]$$

$$E_p = E_i + \frac{RT}{\alpha_c nF}\left(0.780 + \ln\left(\frac{\sqrt{\frac{D_{MgOH^+}\alpha_c nFv}{RT}}}{k^0}\right)\right) \quad [10]$$

$$\Delta E_p = |E_p - E_{p/2}| = 1.857\frac{RT}{\alpha_c nF} \quad [11]$$

Table II. Electrochemical cleaning procedure between experiments.

Procedure step	Description	Duration (s)
1	Apply anodic stripping potential +0.8 V vs Ag/AgCl	3
2	Hold at open circuit potential	240

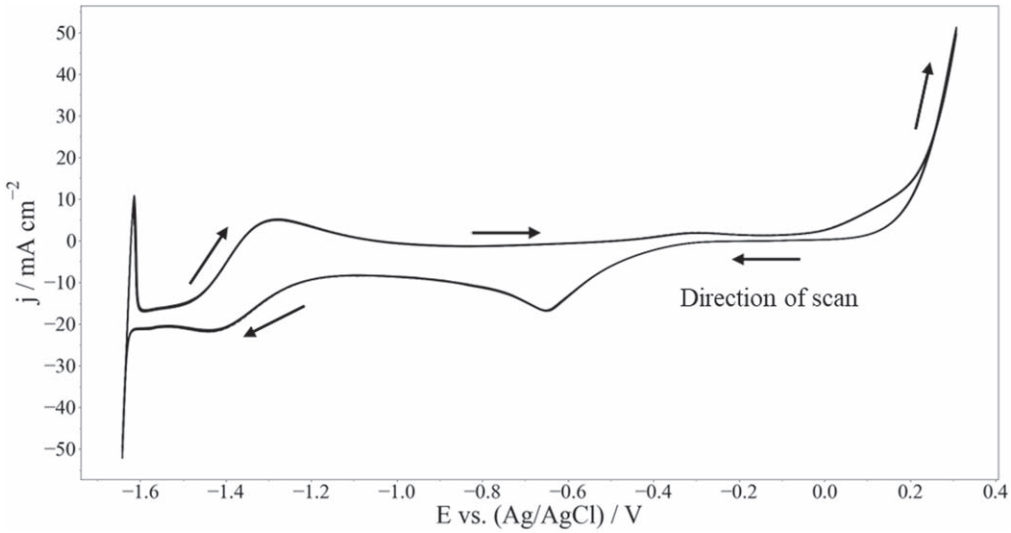

Figure 2. Ten cyclic voltammograms obtained in series at a scan rate of 250 mV s^{-1} and 500 °C.

Table III. Experimentally determined constant for cyclic voltammetry at a scan rate of 250 mV s^{-1} and various temperatures.

Temperature (°C)	$s_{CV}(T, v)$ (ppm O mA^{-1} cm^2)
475	43.7 ± 4.4
500	40.3 ± 2.3
525	37.6 ± 0.3

For an electrochemically quasi-reversible redox reaction the process becomes complicated and relies upon semi-empirical models. Atek et al. derived and experimentally validated the use of Eqs. 12–13 for quasi-reversible systems.

$$-\Phi_{p/2} = 0.770 + \frac{(1.857\alpha_c^{-1} - 0.770)}{1 + \exp\left[\frac{X + (0.557\alpha_c^{-0.216})}{0.445\alpha_c^{0.316}}\right]} \quad [12]$$

Where $\Phi_{p/2}$ is a dimensionless form of $\Delta E_{p/2}$, and X is $\log(\omega)$.

$$\Phi_{p/2} = \frac{nF}{RT}(E_p - E_{p/2}) \quad [13]$$

The utility of Eqs. 5–13 presume uncompensated resistance has been properly accounted for beyond simple subtraction.[44] Otherwise, uncompensated resistance can result in waveform distortion near the redox peaks and mimic the effect of irreversible redox reactions at the electrode.[44,47,48] To attempt to quantify the difference between "true" iR compensation and post-facto compensation the work done by Krulic et al. was followed. First, a dimensionless resistance, ρ_u, needs to be calculated according to Eq. 14:

$$\rho_u = R_u A c_{MgOH^+} \sqrt{\frac{D_{MgOH^+} v (nF)^5}{(RT)^3}} \quad [14]$$

Where R_u is the uncompensated resistance presented earlier (0.1692 Ω), and A is the surface area of the electrode (cm^2).

From Eq. 14, the dimensionless resistance increases with $v^{1/2}$. Therefore, ρ_u(500 °C) was calculated to be 0.65 at the highest scan rate used in this study (2.5 V s^{-1}). The calculations assumed D_{MgOH^+} of 10^{-5} cm^2 s^{-1}, and c_{MgOH^+} of 7×10^{-5} mol cm^{-3} (measured and presented later in this work). This value of ρ was deemed small in the study by Krulic et al., such that post-facto iR compensation via subtraction results in minimal error. The error of peak current, j_p, at 2.5 V s^{-1} is <4%, and the error of peak potential, E_p, is less than 5 mV.[44] Therefore, in this work it was deemed that post-facto iR compensation was appropriate.

Chronopotentiometry for soluble-insoluble reactions.—Sand's equation is commonly employed to determine diffusion coefficients from CP experiments and has been successfully applied to soluble-insoluble reactions in molten salt systems (Eq. 15).[49]

$$j\tau^{1/2} = 0.5nFc_{MgOH^+}\pi^{1/2}D_{MgOH^+}^{1/2} \quad [15]$$

Where τ is the transition time (s).

A plot of j vs $\tau^{-1/2}$ should be linear with an intercept through the origin to indicate a well-behaved system, and E should be constant with respect to applied j to determine reversibility.[49,50] For purely electrochemical reduction reactions (anodic reaction assumed negligible), the shift in E is a function of α_c and can be determined via Eq. 16:[50]

$$E_2 - E_1 = \frac{RT}{\alpha_c F} \ln\left(\frac{j_1}{j_2}\right) \quad [16]$$

Equation 16 is applicable to determine the cathodic charge transfer coefficient, as E shifts with j.[50] For a tenfold increase in applied j, E shifts cathodically by 2.3 $RT/\alpha_c F$.

Square wave voltammetry (SWV) for soluble-insoluble reactions.—A SWV model for soluble-insoluble reactions have been derived by Krulic et al. accounting for uncompensated resistance.[51] This model was experimentally validated in molten salt systems by Fuller et al. to correctly calculate the number of electrons transferred.[52] For a reversible redox reaction Eqs. 17–19 can be employed:

$$w_2 = \frac{W_2 RT}{nF} \quad [17]$$

$$W_2 = 0.7 + 0.3\rho_{u,swv} \quad [18]$$

$$\Delta t = \frac{1}{2f} \quad [19]$$

Where w_2 is the half-width potential of the wave (mV) taken at the back end of the wave, $\rho_{u,swv}$ is the dimensionless uncompensated

resistance for SWV, and f is the frequency employed in SWV (Hz).

$$\rho_{u,swv} = \frac{n^2F^2AR_u c_{MgOH^+}}{RT}\sqrt{\frac{D_{MgOH^+}}{\Delta t}} \quad [20]$$

For irreversible redox reactions, an alternative expression for $\rho_{u,swv}$ is required that accounts for the cathodic charge transfer coefficient. Equation 21 is appropriate in irreversible systems:

$$\rho'_{u,swv} = \frac{\alpha_c nF^2AR_u c_{MgOH^+}}{RT}\sqrt{\frac{D_{MgOH^+}}{\Delta t}} \quad [21]$$

Simple current-time model based on diffusion.—For bulk electrolysis experiments it was interesting to compare experimental data to a simple theoretical model based on diffusion (Eq. 22).

$$j = nF\frac{D_{MgOH^+}c_{MgOH^+}}{\delta} \quad [22]$$

Where δ is the growing diffusion boundary layer. Given the static batch reactor setup in this study, the diffusion boundary layer grows with time according to Eq. 23.

$$\delta = \sqrt{D_{MgOH^+}t} \quad [23]$$

Results and Discussion

Determination of $MgOH^+$ reduction potential.—A baseline CV of the salt is shown in Fig. 3 (1734 ppm $MgOH^+$).

The chloride salt potential window is bounded by Mg reduction occurring at −1.65 V vs Ag/AgCl and chloride oxidation at +0.2 V vs Ag/AgCl. Four peaks are observed in this window, A-D. Skar also observed peaks A-D using a glassy carbon working electrode.[23] Therefore, the peaks are likely inherent to the species within the molten chloride salt. A consensus on the identity of these peaks has previously not been reached. Both Skar and Guo et al. identified peak B as the reduction of $MgOH^+$.[23,35] Skar postulated reaction A to be the reduction of hydrogen ions to hydrogen and observed reactions C and D but provided no further discussion on their origin. Guo et al. assumed reaction C to be the oxidation of hydrogen to H^+ and did not provide discussion around peaks A and D. Conversely, Choi et al. and Ding et al. ascribed peak A to be the reduction of $MgOH^+$.[36,38] Choi et al. also observed peak D, which they reasoned to be the oxidation of O^{2-}. Ding et al. did not further observe peaks B-D. From this discussion the electrochemistry within Mg-K-Na chloride salt is still indeterminant.

To definitively identify the $MgOH^+$ reduction peak, ∼1 g of NaOH was added and compared to the baseline CV as shown in Fig. 4.

After addition of NaOH, the current of peaks A-D all increased. This indicates that peaks A-D are all related to an oxide/hydroxide species in the salt.

To assess peak A, controlled potential coulometry was conducted for 30 min at −0.7 V vs Ag/AgCl. Hydrogen gas was detected 8 min into the experiment and peaked after 16 min (4500 ppm) before gradually declining again. The slow onset of measured H_2 gas product is likely due to the low diffusion coefficient in chloride salts (3.18×10^{-5} cm^2 s^{-1} at 475 °C).[53] However, the low solubility of H_2 in chloride salts ($\kappa_{H_2} = 5.68 \times 10^{-12}$ mol cm^{-3} Pa^{-1}) should result in H_2 simply bubbling away from the melt. The potential for H_2 to absorb to the W electrode is a possible explanation.[53] The length of the tubing did not explain the slow onset either. Further work related to hydrogen gas is suggested for conclusive answers to this behavior. In this work, the gas detector was primarily used to confirm the H_2 as a product from the reduction reaction of peak A. After the 30-minute experiment, the W working electrode was slowly raised out of the salt and analyzed as-is under a SEM with EDS. The SEM image is shown in Fig. 5.

By SEM, a rough and thin deposit layer was observed on the W working electrode. EDS point analysis was conducted at the highlighted region (Fig. 5, right) and shown in Fig. 6.

Elemental analysis indicated the plated species consists of primarily Mg (47.6 atomic %) and O (31.09 atomic %) on the W electrode surface (along with salt residue). Given the atomic % values, MgO was deduced to be the most likely product species on the W electrode surface.

By chemical analysis of the solid product on the W electrode and the gaseous product in the exhaust, peak A was attributed to the reduction of $MgOH^+$ according to Reaction (1). Therefore, for the first time, evidence based on species product analysis has been provided to confirm that the reduction peak at − 0.65 V vs Ag/AgCl corresponds to $MgOH^+$ reduction. For completion, the remainder of this section will attempt to elucidate the reactions for peaks B-D.

To gain further insight into peaks B-D, voltammograms were taken at various scan rates and corrected for uncompensated resistance post-facto (Fig. 7).

The shape of peak A appears to broaden with increasing scan rate and has an atypical response for a single-step reduction reaction. The distortion could be due to the deposition of MgO with subsequent sloughing of MgO or suggests a complex multi-step mechanism.

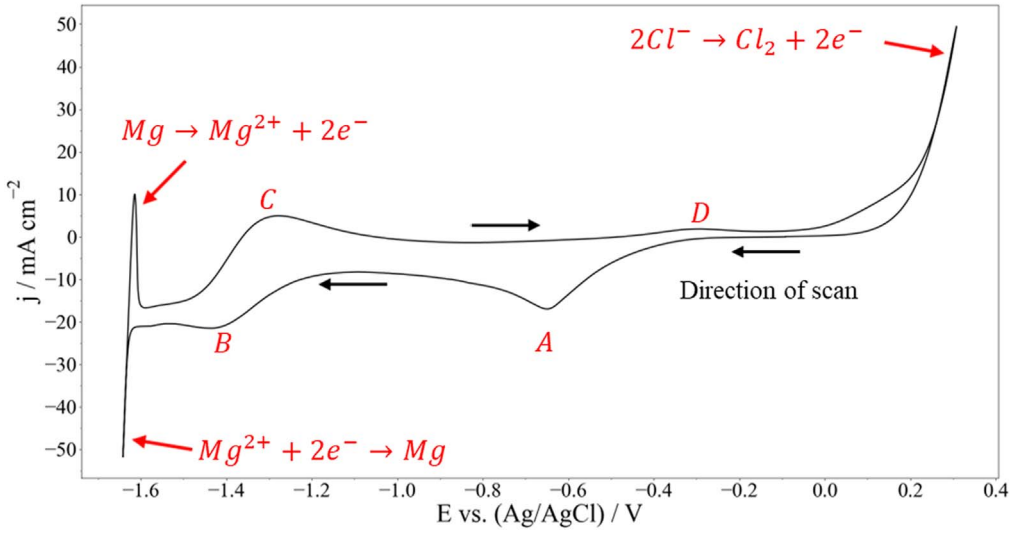

Figure 3. Cyclic voltammogram obtained on W working electrode in chloride mixture at 500 °C and a scan rate of 250 mV s^{-1}.

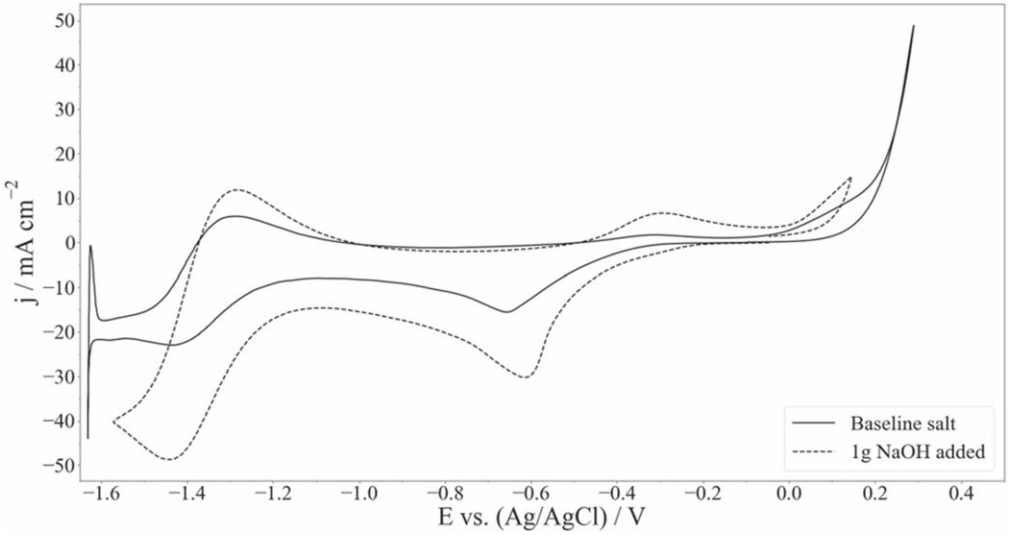

Figure 4. Cyclic voltammogram obtained on W working electrode in chloride mixture at 500 °C and a scan rate of 250 mV s^{-1}. Comparison between voltammogram with and without NaOH addition.

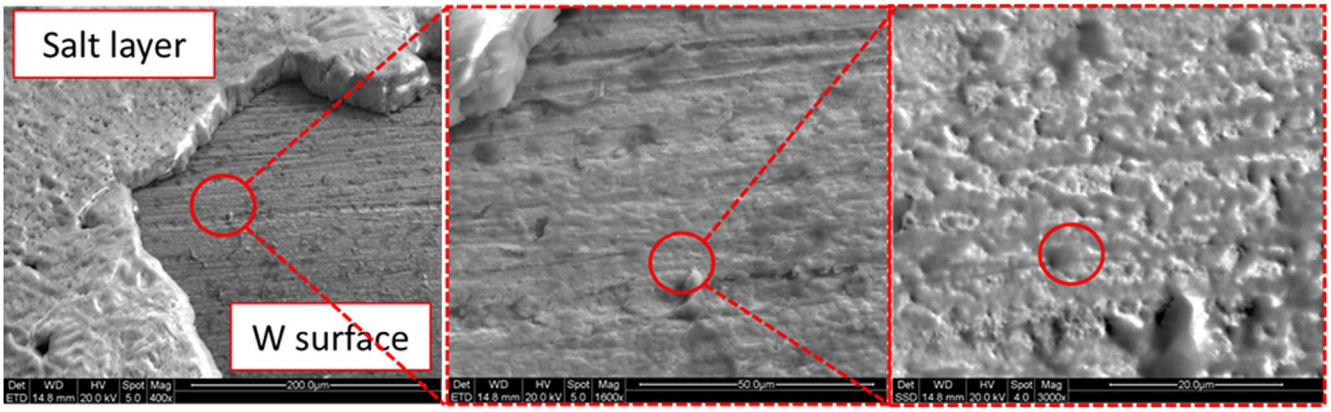

Figure 5. SEM image of W electrode after 30 min of controlled potential coulometry experiment. Left image taken at 400x with red circle highlighting region of zoom in, middle image at 1600x, and right image at 3000x in backscatter mode.

Furthermore, the ΔE_p of 156 mV for peaks B-C agrees well with the theoretical value of 153 mV for a one-electron transfer reversible reaction at 500 °C. This agrees with the work of Guo et al.[35] The peak current densities of A-D were measured with their background currents subtracted and summarized in Table IV.

The current density of peak B matches peak A at a 1–1 ratio above a scan rate of 100 mV s^{-1}. Therefore, peak B is presumed to be a reaction from the product of $MgOH^+$ reduction, either MgO or ½ H_2. MgO is unlikely as its reduction to Mg would be a two-electron transfer reaction. Ito et al. identified the possibility of reducing hydrogen to H^- in molten LiCl-KCl salt.[53] Peak B is plausible to be the reduction of H_2 gas, since at lower scan rates the hydrogen would bubble away and result in lower current densities than peak A. This was observed in our system below a scan rate of 0.1 V s^{-1}. The anodic peak current (peak C) was slightly lower than the cathodic peak current (peak B). This behavior was observed as well in the work conducted by Ito et al.[53] The analysis presented suggests the most plausible explanation for peaks B-C to be hydrogen redox reactions. Choi et al. mentioned the possibility of O^{2-} involved in peak D. A possible reaction is the oxidation reaction of O^{2-} to form OH^-, with the hydrogen coming from reactions A or C. To test, Eq. 6 was used to calculate the current density of peak D at 2.5 V s^{-1} with the following assumptions: concentration of O^{2-} of 50 ppm, diffusion coefficient of 10^{-5} cm^2 s^{-1}, and one electron transferred. A current density of 4.37 mA cm^{-2} was calculated, close to the measured value. The measured value was lower, likely due to the assumptions in the calculation. Alternatively, peak D is the anodic reaction of peak A, and the high potential difference is due to quasi- or irreversibility. This hypothesis was tested by decreasing the switching potential closer and closer to peak A. The anodic response did not change appreciably, so this explanation is unlikely.

Based on species analysis, MgO and H_2 gas were detected from the reduction reaction at −0.65 V vs Ag/AgCl and verified peak A to be reduction of $MgOH^+$. An explanation was given for current behavior of peaks B-D and compared to literature findings suggesting the following set of reactions for each peak:

$$Peak\ A:\ MgOH^+ + e^- \rightarrow MgO + 1/2H_2 \quad [1a]$$

$$Peak\ B:\ 1/2H_2 + e^- \rightarrow H^- \quad [24]$$

$$Peak\ C:\ H^- \rightarrow 1/2H_2 + e^- \quad [25]$$

$$Peak\ D:\ O^{2-} + 1/2H_2 \rightarrow OH^- + e^- \quad [26]$$

Determination of $MgOH^+$ diffusion coefficient, charge transfer coefficient, standard rate constant, and number of electrons transferred.—Before starting the series of experiments at a given

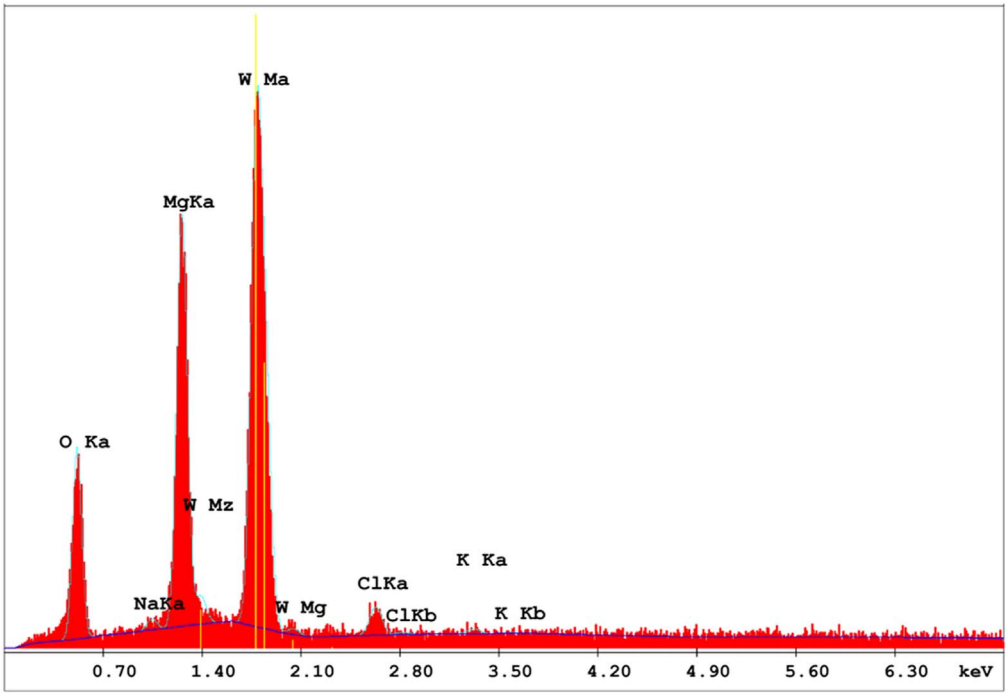

Figure 6. EDS point elemental analysis.

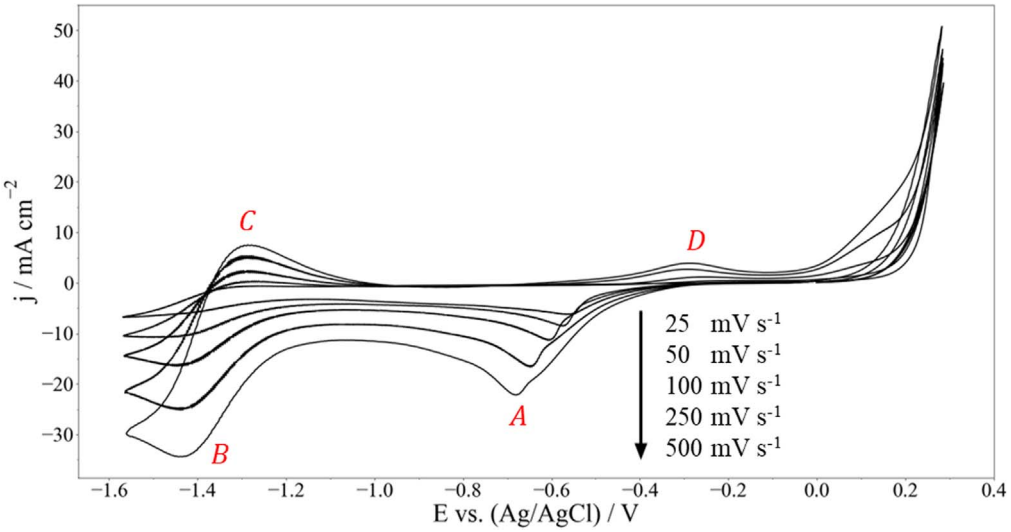

Figure 7. Cyclic voltammogram obtained on W working electrode in chloride mixture at 500 °C and various scan rates.

Table IV. Current density of peaks A-D at various scan rates.

Scan rate	Peak current density			
(V s^{-1})	A (mA cm^{-2})	B (mA cm^{-2})	C (mA cm^{-2})	D (mA cm^{-2})
0.025	6.06	2.77	1.76	0.20
0.05	8.23	6.65	3.18	0.67
0.1	10.94	10.99	9.29	1.44
0.25	16.01	16.70	15.68	1.91
0.5	21.47	23.02	22.64	1.98
0.75	25.45	31.37	27.07	2.78
1	28.82	36.23	34.12	3.21
2.5	44.83	52.20	53.38	3.65

temperature, the bulk concentration of $MgOH^+$ was measured via CV, with the results summarized in Table V.

The variation in concentration measured stems from the uncertainty due to the titration method. Due to this, the average and a 95% confidence interval is reported in Table III. The concentration values from Table V were used in the remainder of the calculations.

To determine reversibility of $MgOH^+$ reduction, CV was employed and a plot of j_p vs $v^{1/2}$ is shown in Fig. 8.

Figure 8 appears to show a linear relationship through the origin between 250 mV s^{-1} and 2.5 V s^{-1}. Typically, this behavior is indicative of either a fully reversible or fully irreversible reaction. However, at low scan rates (25–100 mV s^{-1}) the data appears to deviate from linearity with the overall curve having a slight s-shape and suggests a quasi-reversible reaction. Furthermore, the cathodic shift of E_p with increasing scan rate is typically indicative of a quasi-reversible or irreversible reaction. However, in these molten salt systems, the nucleation and deposit of an insoluble product on a foreign material (MgO on W in this case) also causes shifts in E_p with increasing scan rate.[44,54] Therefore, CP was also employed to assess reversibility.

Chronopotentiograms were recorded between 11 and 12.5 mA and corrected for uncompensated resistance (Fig. 9).

From Fig. 9, a plateau was observed at −0.59 V vs Ag/AgCl corresponding to the reduction of $MgOH^+$ as observed in cyclic voltammograms. A second plateau was observed around −1.35 V vs Ag/AgCl corresponding to the 2nd reduction peak observed in the cyclic voltammogram. It is noteworthy that the potential of the 1st plateau shifts cathodically with increasing current even after correcting for uncompensated resistance. To check for experimental artifacts the transition times were calculated from Fig. 9 and plotted against current densities as shown in Fig. 10.

Figure 10 shows a linear trend with an intercept through the origin for all three temperatures, indicating a well-behaved system.[50] Therefore, Eq. 16 was deemed appropriate to calculate α_c. A value of $\alpha_c = 0.47$ was obtained for all three temperatures. The CP data was also utilized to estimate D_{MgOH^+} using Eq. 15. The average with 95% confidence intervals are tabulated in Table VI.

The obtained values for D_{MgOH^+} appear to not follow an Arrhenius relationship with temperature. However, this interpretation is likely due to the relatively large uncertainty for D_{MgOH^+} at 475 °C. An Arrhenius expression for D_{MgOH^+} is presented in Eq. 27, however, further work is suggested across a wider range of temperature.

$$D_{MgOH^+}(T) = 6.88 \times 10^{-5} \cdot \exp\left(\frac{-17,078}{RT}\right) \quad [27]$$

With D_{MgOH^+} and α_c known Eqs. 12–13 were utilized to determine the reversibility factor (ω). At 500 °C, values of $\omega = 1.4 - 0.3$ are obtained between 0.025–2.5 V s^{-1}. This suggests that $MgOH^+$ reduction is an electrochemically quasi-reversible reaction as expected based on the s-shape behavior in CV (Fig. 8). It is worth emphasizing the necessity of utilizing multiple electroanalytical techniques in molten salt systems to ensure subtle complexities are not overlooked. Furthermore, the use of working plots by calculating the reversibility factor is emphasized for complex molten salt systems.

Table V. Bulk concentration of $MgOH^+$ at each temperature measured via CV.

Temperature (°C)	c_{MgOH^+} (ppm)
475	1802 ± 182
500	1734 ± 97
525	1159 ± 10

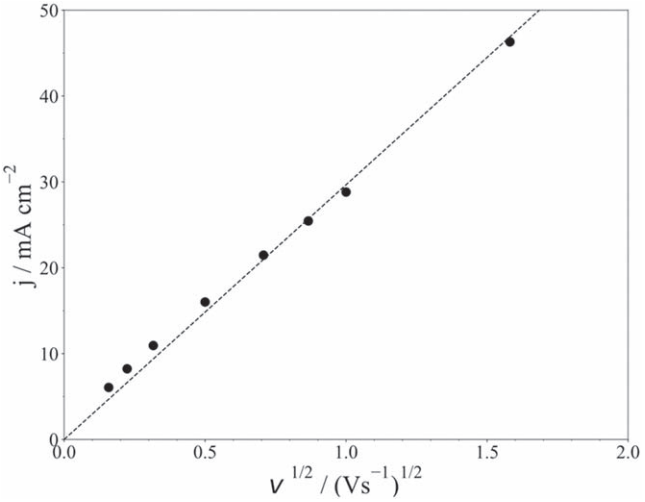

Figure 8. j_p vs $v^{1/2}$ from 25 mV s^{-1} to 2.5 V s^{-1} at 500 °C.

Using the data for α_c and D_{MgOH^+} obtained via CP, Eq. 5 was used to calculate k^0 at various temperatures. The average and 95% confidence intervals are tabulated in Table VII and an Arrhenius expression is derived in Eq. 28.

$$k^0(T) = 1.17 \times 10^{-2} \cdot \exp\left(\frac{-36,060}{RT}\right) \quad [28]$$

The measured values for k^0 were on the order of 10^{-5} cm s^{-1}, typically ascribed to a slow charge transfer reaction, likely due to the energy required for MgO nucleation. Values for metal deposition in molten salt systems are typically one order of magnitude greater such as the case for Mg reduction in chloride salts.[55]

So far, the analysis conducted assumed a single electron transfer ($n = 1$). To verify, SWV was employed. Square-wave voltammograms were recorded between 10 and 20 Hz at 500 °C and shown in Fig. 11.

From Fig. 11, the square-wave voltammograms show a single reduction wave with E_p increasing with frequency. This indicates a single step electron transfer reaction for $MgOH^+$.[56] The atypical CV response for peak A from Fig. 7 is therefore likely due to the nucleation and deposition phenomenon of MgO. Further work is suggested to study this phenomenon.

The work by Krulic et al. did not describe the theory of quasi-reversible reactions for SWV. Given the relatively slow charge transfer kinetics, the theory for irreversible reactions was deemed most appropriate. Using the $E_{p/2}$ obtained at each frequency, and the value of $\alpha = 0.47$ obtained through CP, the value of n was 0.49 ± 0.02, i.e. $n = 1$ when rounded up to the nearest integer. This confirms the reduction of $MgOH^+$ as written in Reaction (1) and confirms the assumption in the previous analysis. With Reaction (1) as written verified and all the parameters obtained, bulk electrolysis experiments were conducted to assess the extent of passivation.

Determination of W passivation from CPC.—With the reduction potential of $MgOH^+$ determined, it is necessary to determine the extent of electrode passivation due to MgO. Ding et al. observed that the current quickly diminished and reached a steady value when electrowinning $MgOH^+$ on a W cathode.[26] The behavior was attributed to W passivation due to MgO. In this work, similar current behavior was observed, as illustrated in Fig. 12. To generate this plot, $MgOH^+$ was introduced into the salt by adding ∼0.25 g NaOH and then a controlled potential coulometry experiment was conducted at −0.7 V vs Ag/AgCl for 30 min while measuring current and cumulative charge transferred.

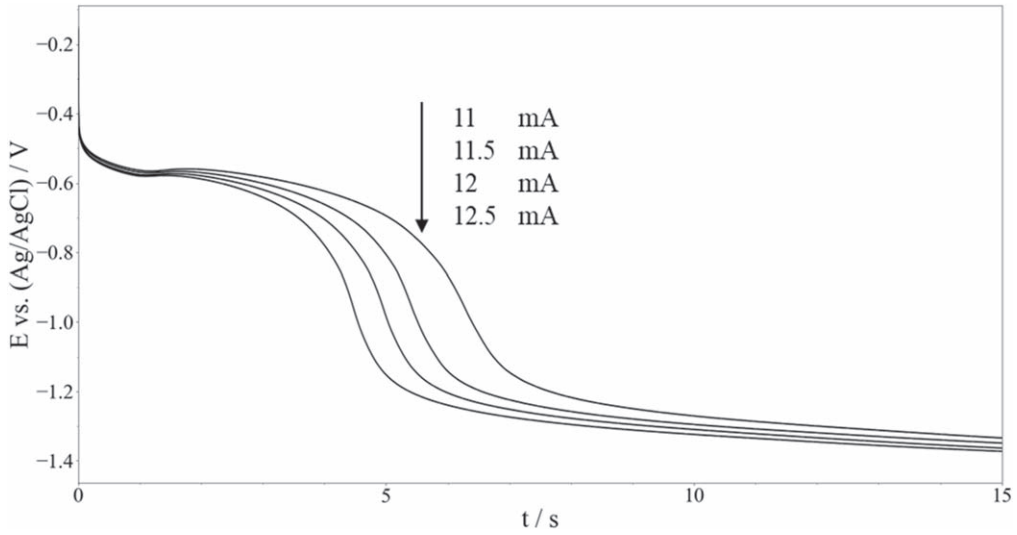

Figure 9. Chronopotentiograms at various currents and 500 °C.

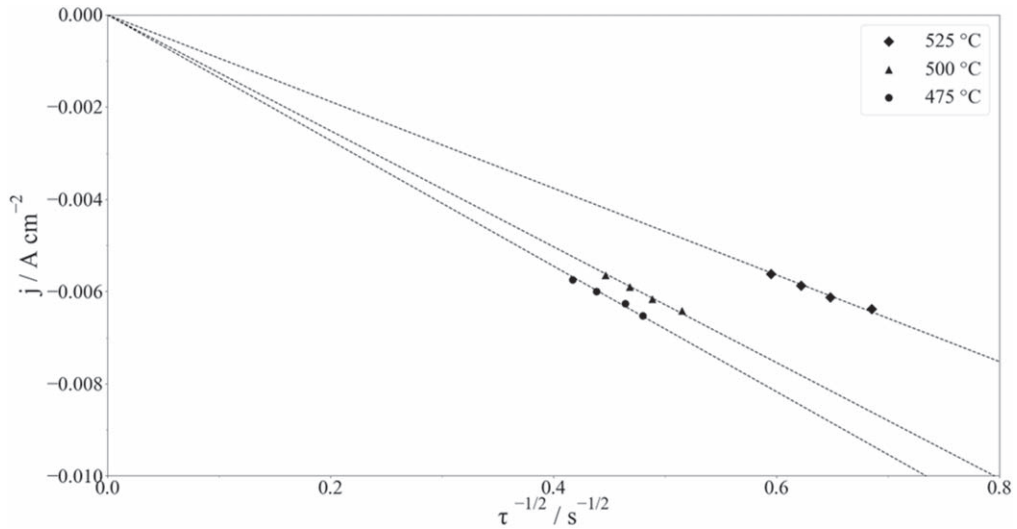

Figure 10. Current densities vs square root of transition times at various temperatures.

Table VI. Measured D_{MgOH^+} at various temperatures.

Temperature (°C)	D^{+}_{MgOH} (CP) $10^6 \times$ (cm^2 s^{-1})
475	4.66 ± 1.54
500	4.36 ± 0.79
525	5.55 ± 0.15

Table VII. Measured k^0 for $MgOH^+$ reduction at various temperatures.

Temperature (°C)	k^0 (CV) $10^5 \times$ (cm s^{-1})
475	3.56 ± 0.72
500	4.25 ± 0.61
525	5.12 ± 1.67

The current density dropped quickly within the first 5 min of the experiment, after which it reached a value of 5 mA cm^{-2}. The current behavior was modeled assuming a diffusion limited process using Eqs. 22–23 for comparison. The concentration of $MgOH^+$ was 2302 ppm (baseline salt + theoretical amount of $MgOH^+$ added from NaOH) and diminished based on the charge passed. The results are shown in Fig. 13.

The simple diffusion limited model underpredicts the measured current. This is likely due to hydrogen evolution causing localized stirring of the solution so that the diffusion boundary layer is smaller than predicted for a completely static solution. The extent of passivation was therefore difficult to determine using the simple diffusion model. A simple stir test was conducted in a new batch of salt where the solution was manually stirred at 5 and 15 min into the experiment. Stirring was done for ∼10 s each time and the current response is shown in Fig. 14.

The effect of stirring is noticeable based on the immediate increase in current density before falling back to baseline again. Based on the observations in both experiments, it is plausible that MgO deposit on the electrode is not strongly adhering and sloughs off in a convective system. To assess this claim, a final experiment was conducted in the same batch of salt. This time ∼1 g of NaOH was added and the CPC experiment was extended to two hours. The electrode was slowly removed from the salt for analysis via SEM-EDS. Figure 15 shows the SEM image of the surface of the W electrode after 2 h of CPC.

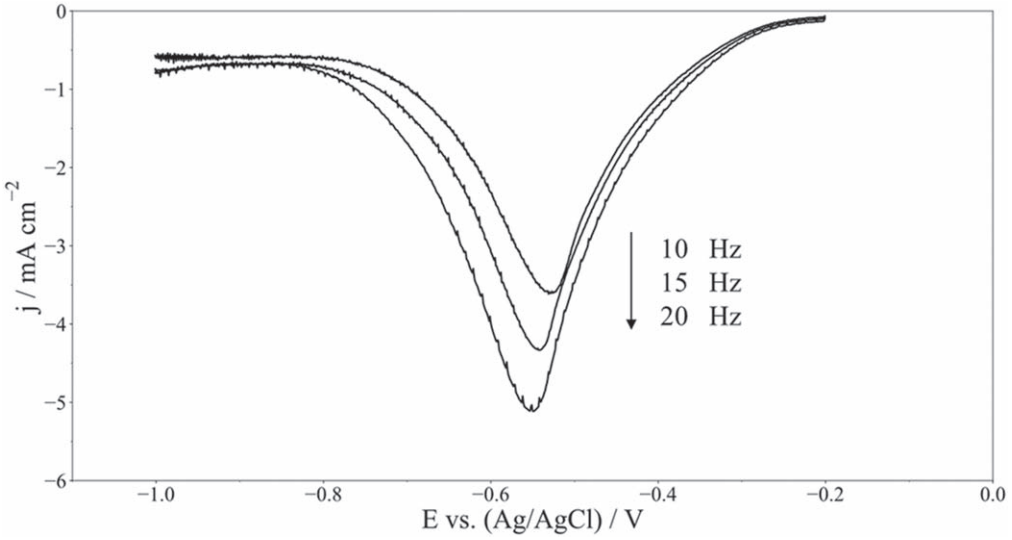

Figure 11. Square-wave voltammograms at various frequencies with a step size of 1 mV and pulse size of 25 mV at 500 °C.

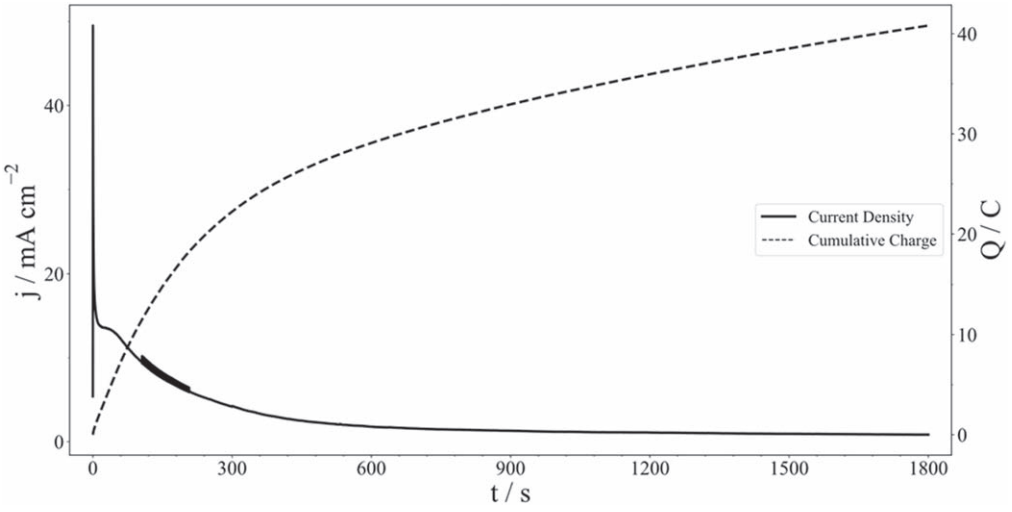

Figure 12. Current density and cumulative charge vs time during controlled potential coulometry at −0.7 V vs Ag/AgCl and 500 °C.

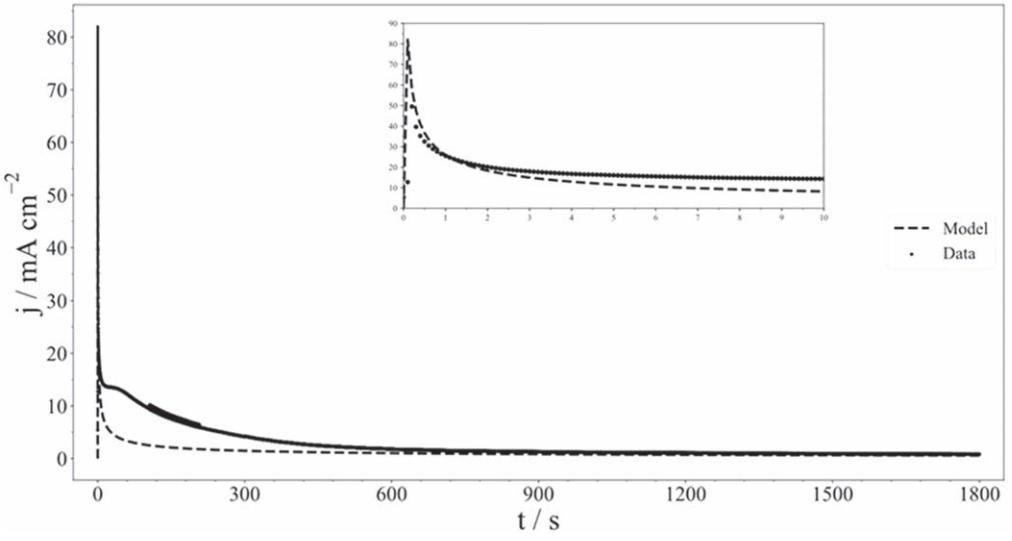

Figure 13. Diffusion controlled current modeling compared to controlled potential coulometry experiment at −0.7 V vs Ag/AgCl and 500 °C.

The light and dark phase in the image correspond to W and MgO respectively. This was confirmed via EDS point analysis, and the elemental results shown in Fig. 16.

The elemental analysis shows the dark phase is primarily Mg and O, with some salt residue and W signal from the electrode. A globular-like deposit of MgO is observed that partially covers the electrode surface, with particle sizes varying from 10–20 μm. Further work is suggested to analyze the salt for MgO particles. By analyzing the particle sizes of MgO in the salt, it would be possible to estimate the critical point for when the deposit becomes too large and sloughs off the electrode. Furthermore, the findings highlight the complexities of this molten salt system where an insoluble product is formed with subsequent sloughing—a phenomenon that the models used in this study do not capture. Further model refinement is suggested to better capture the complex sloughing phenomenon.

The results from this work suggest that in a convective system passivation could be minimized as the salt flow "washes" away the MgO from the electrode surface. Other methods such as pulsing could be employed to try and remove the MgO deposit.[26]

Conclusions

For the first time, the reduction potential of $MgOH^+$ was verified at −0.65 V vs Ag/AgCl in molten Mg-K-Na chloride salt. CV, CP, and SWV were utilized and determined the reduction of $MgOH^+$ to be a single-step, one-electron, quasi-reversible reaction. Furthermore, working curves to assess reversibility were developed based on the procedure from Atek et al. and Krulic et al. The importance of employing these working curves was highlighted since subtleties such as nucleation of an insoluble product on a foreign substrate could easily be overlooked by only analyzing j_p vs $v^{1/2}$ plots, leading to misinterpretation of the reaction mechanism. The charge transfer coefficient, diffusion coefficients, and standard rate constants were measured and presented for the first time in literature.

Bulk electrolysis experiments were performed and determined only partial passivation of the electrode surface. The MgO deposit was hypothesized to be loosely adhering and likely to slough of once a critical mass or size was reached. Scaling up the process to a convective system would be favorable to aid in removal of the MgO deposit.

Further work was suggested to assess the hydrogen redox chemistry in molten chloride salts as well as studying the nucleation phenomenon of MgO on metal electrodes such as W. Further model refinement was also suggested to better capture the phenomenon of sloughing of an insoluble product.

These results can be leveraged for future design and scaling of reactor models to suit industrial needs in CSP and nuclear power plant applications. Future work is planned to assess the kinetics of $MgOH^+$ removal under different overpotentials and pulse techniques to minimize passivation.

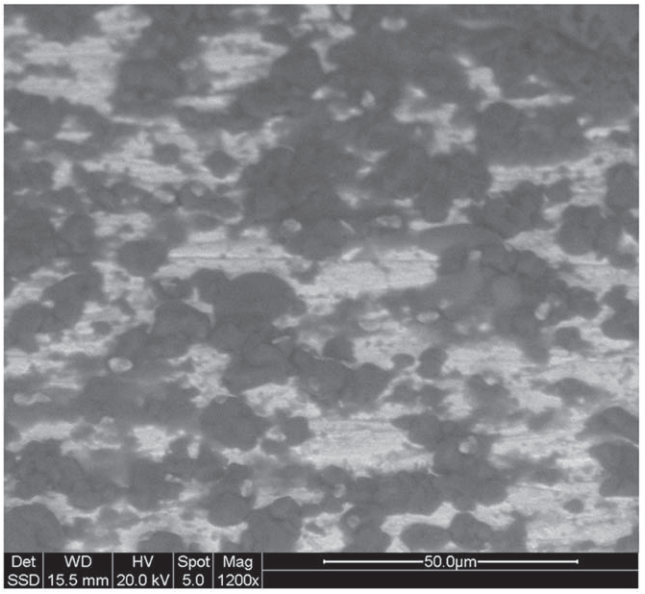

Figure 15. SEM image of W surface after CPC experiment in backscatter mode.

Acknowledgments

This work was authored in part by the National Renewable Energy Laboratory, operated by Alliance for Sustainable Energy, LLC, for the U.S. Department of Energy (DOE) under Contract No. DE-AC36–08GO28308. Funding provided by U.S. Department of Energy Office of Energy Efficiency and Renewable Energy Solar Energy Technologies Office grant CSP #35931 as well as the Colorado School of Mines/NREL Advanced Energy Systems Graduate Program. The views expressed in the article do not necessarily represent the views of the DOE or the U.S. Government. The U.S. Government retains and the publisher, by

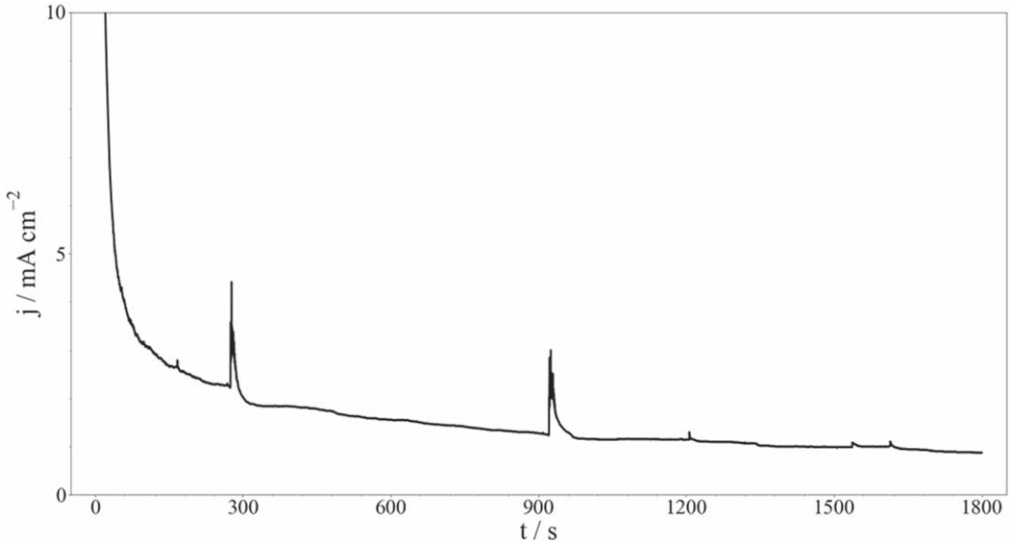

Figure 14. Current density vs time in a simple stir test during controlled potential coulometry at −0.7 V vs Ag/AgCl and 500 °C.

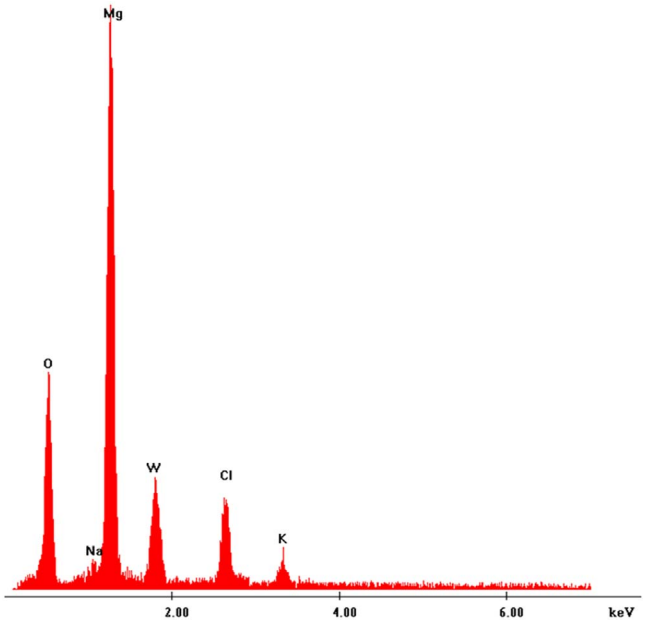

Figure 16. EDS point elemental analysis of dark phase.

ORCID

Liam Witteman https://orcid.org/0000-0001-8450-8263
Kerry Rippy https://orcid.org/0000-0001-7154-6543
Judith Vidal https://orcid.org/0000-0002-0591-3250

References

1. G. Mohan, M. B. Venkataraman, and J. Coventry, "Sensible energy storage options for concentrating solar power plants operating above 600 °C." *Renew. Sustain. Energy Rev.*, **107**, 319 (2019).
2. M. Liu, N. H. Steven Tay, S. Bell, M. Belusko, R. Jacob, G. Will, W. Saman, and F. Bruno, "Review on concentrating solar power plants and new developments in high temperature thermal energy storage technologies." *Renew. Sustain. Energy Rev.*, **53**, 1411 (2016).
3. W. Ding and T. Bauer, "Progress in research and development of molten chloride salt technology for next generation concentrated solar power plants." *Engineering*, **7**, 334 (2021).
4. M. Lambrecht, M. T. de Miguel, M. I. Lasanta, and F. J. Pérez, "Past research and future strategies for molten chlorides application in concentrated solar power technology." *Sol. Energy Mater. Sol. Cells*, **237**, 111557 (2022).
5. A. G. Fernández, J. Gomez-Vidal, E. Oró, A. Kruizenga, A. Solé, and L. F. Cabeza, "Mainstreaming commercial CSP systems: a technology review." *Renew Energy*, **140**, 152 (2019).
6. M. Anderson, K. Sridharan, T. Allen, and P. Peterson, *Liquid Salt Heat Exchanger Technology for VHTR Based Applications*, (Reactor Concepts RD&D) (2012).
7. M. Taube, *Fast Reactors Using Molten Chloride Salts as Fuel* (1978).
8. K. Vignarooban, X. Xu, A. Arvay, K. Hsu, and A. M. Kannan, "Heat transfer fluids for concentrating solar power systems - a review." *Appl. Energy*, **146**, 383 (2015).
9. S. Guo, J. Zhang, W. Wu, and W. Zhou, "Corrosion in the molten fluoride and chloride salts and materials development for nuclear applications." *Prog. Mater Sci.*, **97**, 448 (2018).
10. R. Serrano-López, J. Fradera, and S. Cuesta-López, "Molten salts database for energy applications." *Chemical Engineering and Processing: Process Intensification*, **73**, 87 (2013).
11. S. Ladkany, W. Culbreth, and N. Loyd, "Molten salts and applications III: worldwide molten salt technology developments in energy production and storage." *Journal of Energy and Power Engineering*, **12**, 533 (2018).
12. M. S. Sohal, M. A. Ebner, P. Sabharwall, and P. Sharpe, *Engineering Database of Liquid Salt Thermophysical and Thermochemical Properties* (2010).
13. W. Ding, A. Bonk, and T. Bauer, "Molten chloride salts for next generation CSP plants: selection of promising chloride salts & study on corrosion of alloys in molten chloride salts." *SOLARPACES 2018: International Conference on Concentrating Solar Power and Chemical Energy Systems*, *SOLARPACES*, Casablanca, MoroccoOctober 2-5 (AIP, Casablanca, Morocco) 2126 (2019).
14. C. Villada, W. Ding, A. Bonk, and T. Bauer, "Engineering molten MgCl2–KCl–NaCl salt for high-temperature thermal energy storage: review on salt properties and corrosion control strategies." *Sol. Energy Mater. Sol. Cells*, **232**, 111344 (2021).
15. C. Turchi et al., *CSP Gen3: Liquid-Phase Pathway to SunShot.* (2021).
16. X. Wang, J. D. Rincon, P. Li, Y. Zhao, and J. Vidal, "Thermophysical properties experimentally tested for NaCl-KCL-MgCl2eutectic molten salt as a next-generation high-temperature heat transfer fluids in concentrated solar power systems." *Journal of Solar Energy Engineering*, **143**, 0410054 (2021).
17. S. Kashani-Nejad, *Oxides in the dehydration of magnesium chloride hexahydrate*, McGill University (2005).
18. J. S. C. de Bakker, *The recovery of magnesium oxide and hydrogen chloride from magnesium chloride brines and molten salt hydrates*, Queens's University (2011).
19. N. Klammer, C. Engtrakul, Y. Zhao, Y. Wu, and J. Vidal, "Method to determine MgO and MgOHCl in chloride molten salts." *Anal. Chem.*, **92**, 3598 (2020).
20. W. Ding, H. Shi, Y. Xiu, A. Bonk, A. Weisenburger, A. Jianu, and T. Bauer, "Hot corrosion behavior of commercial alloys in thermal energy storage material of molten MgCl2/KCl/NaCl under inert atmosphere." *Sol. Energy Mater. Sol. Cells*, **184**, 22 (2018).
21. J. C. Gomez-Vidal and R. Tirawat, "Corrosion of alloys in a chloride molten salt (NaCl-LiCl) for solar thermal technologies." *Sol. Energy Mater. Sol. Cells*, **157**, 234 (2016).
22. B. Liu, X. Wei, W. Wang, J. Lu, and J. Ding, "Corrosion behavior of Ni-Based alloys in molten NaCl-CaCl2-MgCl2 eutectic salt for concentrating solar power." *Sol. Energy Mater. Sol. Cells*, **170**, 77 (2017).
23. R. A. Skar, *Chemical and Electrochemical Characterisation of Oxide/Hydroxide Impurities in the Electrolyte for Magnesium Production*, Norges Teknisk-Naturvitenskapelige Universitet (2001).
24. J. M. Kurley, P. W. Halstenberg, A. McAlister, S. Raiman, S. Dai, and R. T. Mayes, "Enabling chloride salts for thermal energy storage: implications of salt purity." *RSC Adv.*, **9**, 25602 (2019).
25. M. Mehos, C. Turchi, J. Vidal, M. Wagner, Z. Ma, C. Ho, W. Kolb, C. Andraka, and A. Kruizenga, *Concentrating Solar Power Gen3 Demonstration Roadmap* (2017).
26. W. Ding, J. Gomez-Vidal, A. Bonk, and T. Bauer, "Molten chloride salts for next generation CSP plants: electrolytical salt purification for reducing corrosive impurity level." *Sol. Energy Mater. Sol. Cells*, **199**, 8 (2019).
27. T. C. Ong, M. Sarvghad, K. Lippiatt, L. Griggs, H. Ryan, G. Will, and T. A. Steinberg, "Review of the solubility, monitoring, and purification of impurities in molten salts for energy storage in concentrated solar power plants." *Renew. Sustain. Energy Rev.*, **131**, 110006 (2020).
28. Y. Zhao, N. Klammer, and J. Vidal, "Purification strategy and effect of impurities on corrosivity of dehydrated carnallite for thermal solar applications." *RSC Adv.*, **9**, 41664 (2019).
29. Y. Zhao and J. Vidal, "Potential scalability of a cost-effective purification method for MgCl2-containing salts for next-generation concentrating solar power technologies." *Sol. Energy Mater. Sol. Cells*, **215**, 110663 (2020).
30. W. Ding, H. Shi, A. Jianu, Y. Xiu, A. Bonk, A. Weisenburger, and T. Bauer, "Molten chloride salts for next generation concentrated solar power plants: mitigation strategies against corrosion of structural materials." *Sol. Energy Mater. Sol. Cells*, **193**, 298 (2019).
31. W. Ding, F. Yang, A. Bonk, and T. Bauer, "Molten chloride salts for high-temperature thermal energy storage: continuous electrolytic salt purification with two Mg-electrodes and alternating voltage for corrosion control." *Sol. Energy Mater. Sol. Cells*, **223**, 110979 (2021).
32. K. Hanson, K. M. Sankar, P. F. Weck, J. K. Startt, R. Dingreville, C. S. Deo, J. D. Sugar, and P. M. Singh, "Effect of excess Mg to control corrosion in molten MgCl2 and KCl eutectic salt mixture." *Corros. Sci.*, **194**, 109914 (2022).
33. H. Sun, J. Q. Wang, Z. Tang, Y. Liu, and C. Wang, "Assessment of effects of Mg treatment on corrosivity of molten NaCl-KCl-MgCl2 salt with Raman and infrared spectra." *Corros. Sci.*, **164**, 108350 (2020).
34. Y. Zuo, Y. L. Song, R. Tang, and Y. Qian, "A novel purification method for fluoride or chloride molten salts based on the redox of hydrogen on a nickel electrode." *RSC Adv.*, **11**, 35069 (2021).
35. J. Guo, N. Hoyt, and M. Williamson, "Multielectrode array sensors to enable long-duration corrosion monitoring and control of concentrating solar power systems." *J. Electroanal. Chem.*, **884**, 115064 (2021).
36. W. Ding, A. Bonk, J. Gussone, and T. Bauer, "Cyclic voltammetry for monitoring corrosive impurities in molten chlorides for thermal energy storage." *Energy Procedia*, **135**, 82 (2017).
37. Q. Gong, H. Shi, Y. Chai, R. Yu, A. Weisenburger, D. Wang, A. Bonk, T. Bauer, and W. Ding, "Molten chloride salt technology for next-generation CSP plants: compatibility of Fe-Based alloys with purified molten MgCl2-KCl-NaCl salt at 700 °C." *Appl. Energy*, **324**, 119708 (2022).
38. S. Choi, N. E. Orabona, O. R. Dale, P. Okabe, C. Inman, and M. F. Simpson, "Effect of Mg dissolution on cyclic voltammetry and open circuit potentiometry of molten MgCl2–KCl–NaCl candidate heat transfer fluid for concentrating solar power." *Sol. Energy Mater. Sol. Cells*, **202**, 110087 (2019).
39. H. Wang, N. J. Siambun, L. Yu, and G. Z. Chen, "A robust alumina membrane reference electrode for high temperature molten salts." *J. Electrochem. Soc.*, **159**, H740 (2012).
40. N. Elgrishi, K. J. Rountree, B. D. McCarthy, E. S. Rountree, T. T. Eisenhart, and J. L. Dempsey, "A practical Beginner's guide to cyclic voltammetry." *J. Chem. Educ.*, **95**, 197 (2018).

41. D. Rappleye, D. Horvath, Z. Wang, C. Zhang, and M. F. Simpson, "Methods for determining the working electrode interfacial area for electroanalytical measurements of metal ions in molten LiCl-KCl." *ECS Trans.*, **75**, 79 (2016).
42. M. M. Tylka, J. L. Willit, J. Prakash, and M. A. Williamson, "Method development for quantitative analysis of actinides in molten salts." *J. Electrochem. Soc.*, **162**, H625 (2015).
43. I. Atek, S. Maye, H. H. Girault, A. M. Affoune, and P. Peljo, "Semi-analytical modelling of linear scan voltammetric responses for soluble-insoluble system: the case of metal deposition." *J. Electroanal. Chem.*, **818**, 35 (2018).
44. D. Krulic, N. Fatouros, and D. Liu, "A complementary survey of staircase voltammetry with metal ion deposition on macroelectrodes." *J. Electroanal. Chem.*, **754**, 30 (2015).
45. T. Berzins and P. Delahay, "Oscillographic polarographic waves for the reversible deposition of metals on solid electrodes." *J. Am. Chem. Soc.*, **75**, 555 (1953).
46. P. Delahay, "Theory of irreversible waves in oscillographic polarography." *J. Am. Chem. Soc.*, **75**, 1190 (1953).
47. T. Williams, R. Shum, and D. Rappleye, "Review—concentration measurements in molten chloride salts using electrochemical methods." *J. Electrochem. Soc.*, **168**, 123510 (2021).
48. E. J. F. Dickinson, J. G. Limon-Petersen, N. V. Rees, and R. G. Compton, "How much supporting electrolyte is required to make a cyclic voltammetry experiment quantitatively "diffusional"? a theoretical and experimental investigation." *J. Phys. Chem. C*, **113**, 11157 (2009).
49. H. Tang and B. Pesic, "Electrochemical behavior of LaCl3 and morphology of La deposit on molybdenum substrate in molten LiCl-KCl eutectic salt." *Electrochim. Acta*, **119**, 120 (2014).
50. A. J. Bard and L. R. Faulkner, *Electrochemical Methods: Fundamentals and Applications* (Wiley, New Jersey) (1944).
51. D. Krulic and N. Fatouros, "Peak heights and peak widths at half-height in square wave voltammetry without and with ohmic potential drop for reversible and irreversible systems." *J. Electroanal. Chem.*, **652**, 26 (2011).
52. R. Fuller, T. Williams, M. Schvaneveldt, and D. Rappleye, "A comparison of square-wave voltammetry models to determine the number of electrons exchanged in metal deposition." *Electrochim. Acta*, **414**, 140220 (2022).
53. H. Ito and Y. Hasegawa, "Electrode Behavior of Hydrogen Reduction in LiCl-KCl Melt Voltammetric Analysis." *J. Electrochem. Soc.*, **147**, 289 (2000).
54. N. C. Hoyt, J. L. Willit, and M. A. Williamson, "Communication—quantitative voltammetric analysis of high concentration actinides in molten salts." *J. Electrochem. Soc.*, **164**, H134 (2017).
55. B. Borresen, G. M. Haarberg, and R. Tunold, "Electrodeposition of magnesium from halide melts-charge transfer and diffusion kinetics." *Electrochim. Acta*, **42**, 1613 (1997).
56. J. G. Osteryoung and R. A. Osteryoung, "Square wave voltammetry." *Anal. Chem.*, **57**, 101 (1985).